

Stoichiometric effects on the photoelectric properties of LiInSe₂ crystals for neutron detection

Lijian Guo^{1, 2, 3}, Yadong Xu^{1, 2, 3}, Hongjian Zheng^{1, 2}, Wangqi Xue^{1, 2}, Jiangpeng Dong^{1, 2}, Binbin Zhang^{1, 2}, Yihui He³, Gangqiang Zha^{1, 2}, Duck Young Chung⁴, Wanqi Jie^{1, 2}, Mercuri G. Kanatzidis^{3, 4*}*

¹State Key Laboratory of Solidification Processing and ²Key Laboratory of Radiation Detection Materials and Devices, Northwestern Polytechnical University, Xi'an 710072, China

³Department of Chemistry, Northwestern University, Evanston, IL 60208, USA

⁴Materials Science Division, Argonne National Laboratory, Argonne, IL 60439, USA

ABSTRACT

⁶LiInSe₂ is a promising semiconductor candidate for thermal neutron detection due to its large capture cross-section. However, the charge collection efficiency is still insufficient for high resolution for the grown-in defects induced by the stoichiometric deviation. In this work, we report photoelectric properties of stoichiometric LiInSe₂ crystal boules up to 70mm in length and 20mm in diameter grown by the vertical Bridgman method. Inductively Coupled Plasma (ICP) measurements demonstrate the ratio of Li, In and Se of the as-grown crystal is very close to 1: 1: 2, which is optimized by low temperature synthesis processing. The obtained single crystals display high bulk resistivity in the range of 10¹¹-10¹² Ω·cm and a direct band gap of 2.01 eV - 2.83 eV with a changeable color from red to yellow. The electronic structure of LiInSe₂ was studied using first-principles density functional theory (DFT) calculations, which predicts that the anti-site defects of In_{Li} and Li_{In} are the dominant factor for the different crystal colors observed. The stoichiometric LiInSe₂ crystal gives an improved energy resolution, for a semiconductor detector when illuminated with a ²⁴¹Am@5.48 MeV α source, of 23.3%. The electron mobility-lifetime product ($\mu\tau$) is $\sim 2.5 \times 10^{-5}$ cm²V⁻¹.

Introduction

^3He based gaseous detectors have been used for thermal neutron detection for many years, however, the widespread application is hampered by their large volume and the need to integrate with compact handheld detection instruments. Coupled with potential future shortages of ^3He , which is also of concern makes a significant and compelling case to develop novel neutron detectors¹. Currently, two mainstream categories of thermal neutron detectors are considered. One is the scintillator detector based on the emitted visible light upon absorption of neutrons²⁻⁴, another is the semiconductor detector coated with neutron-active isotopes. The latter is usually composed of thin-film coatings of neutron-active material (or ‘converter foils’) and charge collecting part, such as $^6\text{Li}/^{10}\text{B}$ rich converter foils and Si, GaAs, diamond correspondingly⁵⁻⁸. However, the detection efficiency of the composite-type neutron detectors is determined by the self-absorption effects of the converter foil⁹. By increasing the thickness of the films, the neutron absorption efficiency can be improved, while the charged particles, the products of nuclear reactions, tend to be trapped by the coated converter foils. It is difficult, however, to achieve high efficiency of neutron absorption and charge collection simultaneously in this fashion. Hence, a third type of detector based on homogeneous semiconductor materials which can absorb neutrons and subsequently collect the resulting charge carriers is highly attractive.

LiInSe_2 is a member of I-III-VI chalcogenide family with a large nonlinear optical coefficient and suitable transparent wavelength range that has been studied in the field of nonlinear optics for over a decade¹⁰⁻¹². In recent reports, $^6\text{LiInSe}_2$ crystals exhibit promising ability to respond to ionizing radiation through direct charge carrier transport by the nuclear reaction $^6\text{Li}(n,\alpha)^3\text{H}$ ¹³⁻¹⁵. The density of ^6Li atoms in $^6\text{LiInSe}_2$ crystal is sufficient to ensure > 95% absorption of neutrons in a 3.4mm thick wafer¹⁶.

Since the first reported single crystal growth of LiInSe₂ in 1981, the crystal quality has improved enormously in recent years¹⁷⁻²². However, the charge carrier collection efficiency is still unsatisfactory for high resolution detection due to grown-in defects, such as In_{Li}, Li_{In}, V_{Se}, V_{Li}, Li_i and In_i. The band gap of LiInSe₂ surprisingly appears to vary over a wide range of 1.6 eV-2.86 eV^{17-19,23} at room temperature, with color from red to yellow²⁰. Based on first-principles theoretical calculations, the yellow crystal with a band gap of 2.86 eV at room temperature is predicted to be almost free from the grown-in defects²⁴. The photoluminescence (PL) spectrum at 77 K shows the red crystal even has a higher-energy free exciton emission peak (3.065 eV)²⁵, which is close to the yellow one. In_{Li}^{+1/2+} and Li_{In}^{-1/2-}, reported as the dominant grown-in defects determining the color variation of the crystals, lead to the strong red shift of the absorption edge^{24,25}. V_{Li} and Li_i are thought to be abundant in samples grown from Li-deficient and Li-rich environment respectively²⁴. The cation rich conditions of as-grown crystals are probably responsible for Se vacancies V_{Se}^{17,23}, electron donors in LiInSe₂. Also, it is reasonable to speculate that In_i is likely to be present in In-rich conditions. These defects are closely related to the stoichiometric deviation of LiInSe₂ crystals grown from a melt. Usually, excess Se and Li are added to compensate the loss from evaporation and chemical reaction, but the obtained crystals can still deviate from stoichiometry significantly, resulting Li_{0.88}In_{0.86}Se₂²¹, Li_{0.74}In_{0.92}Se₂²⁶ and Li_{0.91}InSe₂¹⁹. The huge Li stoichiometric deviation, even up to 25%, induces abundant vacancies of lithium V_{Li}. Correspondingly, the carrier mobility-lifetime product ($\mu\tau$) of detectors is relatively low of 3-7.6×10⁻⁶ cm²/V^{16,27}. Therefore, it is still a significant challenge to properly tailor the stoichiometry and the native defects during melt growth.

In order to reduce the stoichiometric deviation of grown LiInSe₂ crystals, in this work, we guided the synthesis of polycrystalline LiInSe₂ at lower temperatures using a relatively slow

heating process. The transmittance, photoresponse, resistivity and alpha particle response of the as-grown stoichiometric LiInSe_2 crystals were characterized. We also discuss the LiInSe_2 detector performance as a function of various conditions such as excess amount of Li and Se and their effect on the stoichiometric deviation. Moreover, the LiInSe_2 detector, as desired, exhibits only a dull response to γ -rays because of its relatively small mean atomic number. We also present first-principles calculations of the electronic structure with new insight on the defect behavior in the crystal structure of this material. We show that the yellow stoichiometric crystal achieves an energy resolution of 23.3% for alpha particles of 5.48 MeV of ^{241}Am source which is an improvement over state of the art. These results impact the strategies for further improvement of LiInSe_2 crystals by controlling the component deviation, engineering the native defects and growing detector-grade crystals.

Experimental Section

The Synthesis of LiInSe_2 Polycrystalline

Polycrystalline LiInSe_2 was synthesized from Li (4N), In (6N) and Se (6N). The element reagents of Li, In and Se were weighed in a 1: 1: 2 stoichiometric ratio with an excess of Li and Se, which was added to compensate the Li lost from the reaction with fused silica and the high Se vapor pressure. The red and yellow crystals of LiInSe_2 will be referred to as LISe-R and LISe-Y respectively.

LISe-R: In an argon-filled glovebox, 2.929 g of Li (with excess 5% Li), 46.143 g of In and 64.745 g Se (with excess 2% Se) were weighed.

LISe-Y: In an argon-filled glovebox, 2.895 g of Li (with excess 3% Li), 46.489 g of In and 65.228 g Se (with excess 2% Se) were weighed.

Then the raw material was loaded into a graphite crucible and sealed in a carbon coated fused silica ampoule under the pressure of 5×10^{-5} Pa. The ampoule was put in a rotating furnace. The system temperature was raised from room temperature to 180 °C (the melting point of Li) rapidly and then increased to 250 °C in 6 hours. After that, the system was soaked at 500 °C, 750 °C and 920 °C separately making the polycrystalline uniform. The furnace was kept at 920 °C and rotated for 24 hours and then cooled 10 °C/h to 700 °C followed by cooling 50 °C/h to room temperature. Finally, the obtained polycrystalline of LISe-R and LISe-Y revealed dark red and yellow respectively.

Crystal Growth

The LiInSe₂ single crystals were grown by a vertical Bridgman method. The raw polycrystalline materials were loaded into crucibles and sealed under the pressure of 5×10^{-5} Pa. The temperature was then raised from room temperature to 950 °C at the rate of 80 °C/h and soaked at the max temperature for 2 hours. Then the crucible was moved to the starting position, and descended at the velocity of 0.5 mm/h. The temperature gradient of 10 °C/cm was realized in the growth region of the furnace. After growth run, the LiInSe₂ crystal was cooled down to ambient temperature at a rate of 5-50 °C/h.

LISe-R1: The polycrystalline samples of LISe-R were subsequently placed into a carbon coated fused silica crucible. The inner diameter of the crucible was 20 mm with a wall of 3 mm. The obtained crystal ingot revealed dark red and a wafer was cut from the crystal named LISe-R1.

LISe-R2: The polycrystalline samples of LISe-Y were loaded into a smaller carbon coated fused silica crucible with an inner diameter of 12 mm. The crystal ingot color in this case was changed to light red instead of the polycrystalline color of yellow. The crystal ingots grown in fused silica crucible were easily removed from the crucible.

LISe-Y: The polycrystalline samples of LISe-Y were loaded into a graphite crucible with an inner diameter of 20 mm. The graphite crucible was inserted into a carbon coated fused silica tube. Finally, a yellow crystal ingot of LISe-Y was obtained, however it was difficult to remove it from the crucible because of interaction with crucible wall. The cut crystal wafers were mechanically lapped with MgO powders mixed in deionized water for the following experiments. The crystals are air- and water-stable, while the surface is easily oxidized in a few days.

Characterization

In order to optimize the synthesis process, differential scanning calorimetry (DSC) analyses were performed on the systems of Li-Se, In-Se and Li-In to confirm the reaction temperature of these raw materials with Netzsch STA-449C thermal analyzer.

SHIMADZU UV-3150 UV-Visible-NIR and Nicolet Nexus Fourier transform infrared spectrometer were used to extract the transmittance spectra at room temperature. The molar ratio of Li, In and Se for as-grown crystals was identified by Optima 8300 Inductively Coupled Plasma (ICP) Optical Emission Spectrometer (OES). The resistivity of LiInSe₂ crystals was measured using an Agilent 4155C Semiconductor Parameter Analyzer. The resistivity was measured with the bias range from -100 V to 100 V. The photoconductivity was performed under the illumination of both ambient light and 365 nm LED light, and recorded by a Keithley 485 picoammeter.

For the characterization of detection properties, Au contacts were evaporated onto both faces of the wafers after polish. Subsequently, passivation of the remaining bare LiInSe₂ surface was performed to minimize the surface leakage current with a 30% H₂O₂ solution. Finally, one face of the detector was bonded by silver paste to a sample holder and the opposite electrode was connected using a Cu wire for further measurements.

Alpha particle response measurement of LiInSe₂ detector was carried out at room temperature using an un-collimated ²⁴¹Am radioactive source producing 5.48 MeV alpha particles. The ²⁴¹Am source was mounted 5 mm above the sample. During the measurement, the sample was connected to a charge sensitive preamplifier from Imdetek Corporation under a bias from a low-noise Ortec 556 high voltage source. The preamplifier output signals were shaped by an Ortec 673 spectroscopy amplifier with a shaping time of 1μs, followed by acquisition of pulse height spectra using an Ortec multi-channel analyzer. For the mobility evaluation, the electron transit time, recording the rise time from the preamplifier instead of transferring to the Ortec 673 amplifier, were collected by an oscilloscope with a resolution of 4 ns. Moreover, the γ response of LiInSe₂ detector was measured under the illumination of a ⁶⁰Co@1.33MeV radioactive source (attached in Supporting Information).

Results and discussion

Low Temperature Synthesis and Crystal Growth

Figure 1 shows that the vapor pressure of Li and Se increase significantly with temperature^{28, 29}. The reported synthesis methods usually employed high initial temperatures, such as 400 °C¹⁷, 500 °C²¹, 600 °C²⁰ or 680 °C²⁶, which likely cause the large stoichiometric deviation. Although

the vapor pressure of Li is lower than Se, the Li loss amount is not negligible given its higher chemical activity at a higher temperature. Unlike Se, Li tends to evaporate constantly from the melt, since the gas-liquid equilibrium continues to break down from the reaction between the Li and silica ampoule. Therefore, to effectively decrease the loss of raw materials, a relatively low temperature for LiInSe₂ synthesis is preferable.

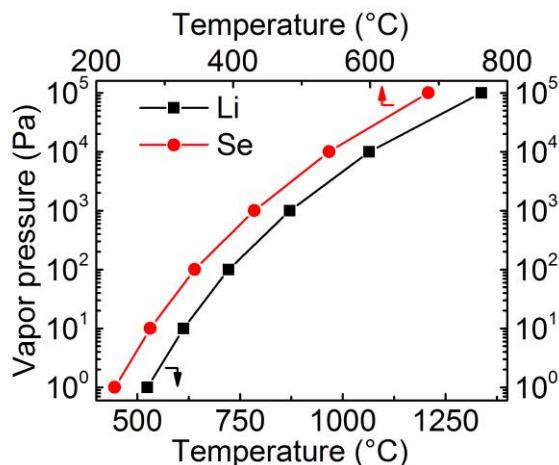


Figure 1. Vapor pressure of Se and Li at various temperatures.

Differential scanning calorimetry (DSC) analyses were performed on the systems of Li-Se, In-Se and Li-In to understand the combination reaction temperatures and optimize the synthesis process. In, Li and Se melt at 157 °C, 184 °C (Peak 1 in Figure 2a) and 220 °C (Peak 2 in Figure 2a) respectively. Compared with the exothermic peaks above 400 °C in the Li-In system (the forming of LiIn, shown in Figure 2c), the intense exothermic peak observed at 220 °C (Peak 3 in Figure 2a) indicates Li reacts with Se immediately when Se melts. The heat produced from the reaction increases the system temperature in a short period of time and leads to continuous reaction. In the In-Se system (Figure 2b), we observed one exothermic peak around 240 °C indicating Se can react with In just above its melting point. Hence, Li₂Se and In_xSe_y (like In₂Se₃, In₂Se, InSe, In₅Se₆) are believed to be obtained below 250 °C in a Li-In-Se reaction system²¹.

Based on these results, we employed a slow heating process of 5-15 °C/h from 180 °C to 250 °C. The prolonged duration ensures the formation of Li_2Se and In_xSe_y , the chemical activity of Li is reduced, and the Se evaporation is suppressed. Then, the system was kept at 500 °C and 750 °C respectively, causing the binary compounds to form the ternary target of LiInSe_2 . The powder XRD patterns of the as-synthesized polycrystalline material show good agreement with the calculated results indicating that the samples are single phases (Figure 3).

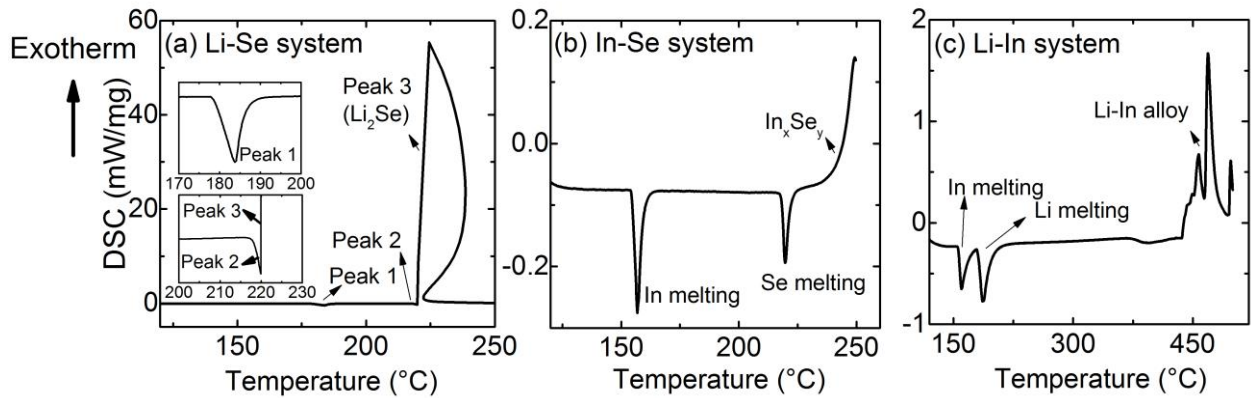


Figure 2. Differential scanning calorimetry results of (a) Li-Se system (see violent exothermal reaction in peak 3 indicating the forming of Li_2Se), (b) In-Se system and (c) Li-In system.

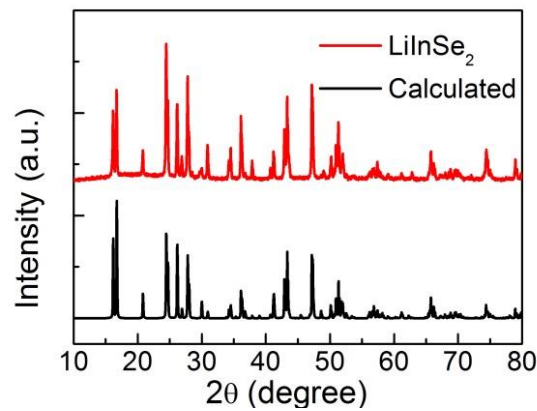


Figure 3. Typical powder XRD patterns of as-synthesized polycrystalline LiInSe_2 .

The crystals were subsequently grown using the synthesized polycrystalline material. Figure 4a and 4b show the grown LiInSe₂ ingots with red (LISE-R) and yellow (LISE-Y) polycrystalline grown in fused silica crucibles. The dimension of wafers LISe-R1, LISe-R2 and LISe-Y are 5×5×2 mm³ (Figure 4c). According to the chemical formulas determined by ICP and listed in Table 1, the as grown crystals are rich in cations. The components are much close to the stoichiometric ratio, thanks to the low temperature synthesis method.

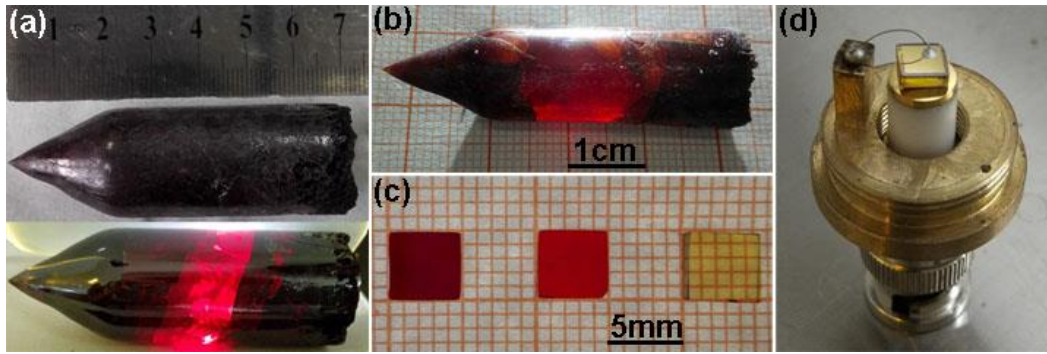


Figure 4. (a) Crystal ingot LISe-R1 grown with excess 5% Li and 2% Se (LISE-R); (b) Crystal ingot LISe-R2 grown with excess 3% Li and 2% Se (LISE-Y); (c) Wafer LISe-R1 (left), LISe-R2 (center) and LISe-Y (right); (d) The fabricated LiInSe₂ detector.

Table 1. Chemical compositions of as-grown and reported LiInSe₂ crystals

Wafer	Excess amount (at. %)	Li (at. %)	In (at. %)	Se (at. %)	Formula
LISe-R1	5% Li, 2% Se	2.48	43.66	54.41	Li _{1.04} In _{1.10} Se ₂
LISe-R2	3% Li, 2%Se	2.40	41.25	55.44	Li _{0.99} In _{1.02} Se ₂
LISe-Y	3% Li, 2%Se	2.41	42.21	54.93	LiIn _{1.06} Se ₂
Ref[19]		2.26	41.13	56.61	Li _{0.91} InSe ₂
Ref[26]		1.92	39.44	58.66	Li _{0.74} In _{0.92} Se ₂
Ref[21]		Li _{0.88} In _{0.86} Se ₂			

Optical Properties and Electronic Structure calculations

The as-grown crystals display various colors, as shown in Figure 4c, from dark red to light red and yellow. Figure 5(a) (transmittance spectra extracted from UV-Vis-NIR) and Figure 5(b) (transmittance spectra extracted from Fourier transform infrared spectrometer) reveal the average transmittance is higher than 70% in the range of 0.8-9 μm for LISe-R1, LISe-R2 and LISe-Y. We derived the optical band gap of as-grown LiInSe₂ by fitting the $(\alpha h\nu)^2$ vs $h\nu$ plot according to Tauc relation (Figure 5c)^{30, 31}, and α is the absorption coefficient. The optical band gap was determined to be 2.01 eV, 2.15 eV and 2.83 eV for LISe-R1, LISe-R2 and LISe-Y, respectively.

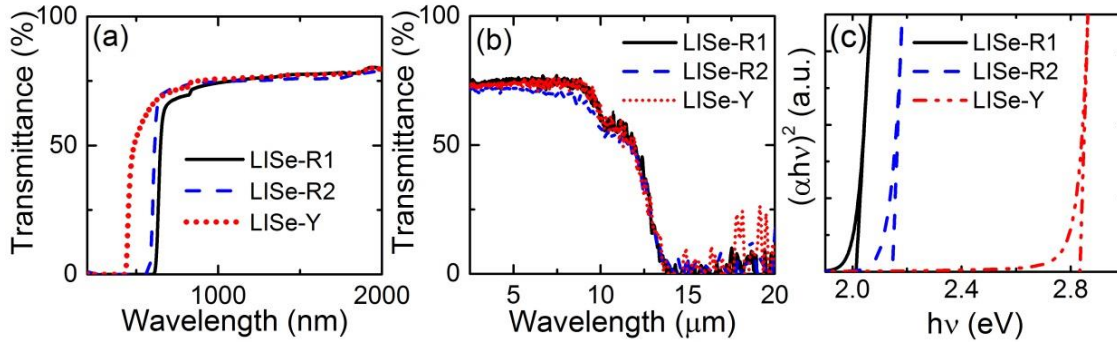


Figure 5. (a) and (b) show the transmittance spectra of LiInSe₂ wafers with different colors, (c) is the plot of $(\alpha h\nu)^2$ vs $h\nu$.

Theoretical calculations of the electronic band structure of LiInSe₂ were carried out using the Vienna Ab-initio Simulation Package (VASP) implementation of Density Functional Theory (DFT) in conjunction with the projector augmented-wave (PAW) formalism³²⁻³⁴. The Perdew-Burke-Ernzerhof generalized gradient approximation (PBE-GGA) was employed for the exchange-correlation potentials³⁵. Figure 6a presents the calculated band structure and shows a direct band gap of 1.612 eV given both valence band maximum (VBM) and conduction band minimum (CBM) located at the Γ point of the Brillouin zone. This is lower than the experimental value of 2.01- 2.83 eV, because the ignorance of excited states leads to the underestimation of band gap³⁶, a well known tendency of this kind of calculations. The contributions of Li, In and

Se to the density of states (DOS) are shown in Figure 6b. The highest occupied crystal orbitals are constructed mainly by the Se-4p, Li-2s and In-5p. Interestingly, Li seems to play a very limited role in the lowest orbitals of the conduction band. The lowest unoccupied crystal orbitals are mainly composed of anti-bonding orbitals of In-5s and Se-4p suggesting that In broadens the conduction band and narrows the band gap.

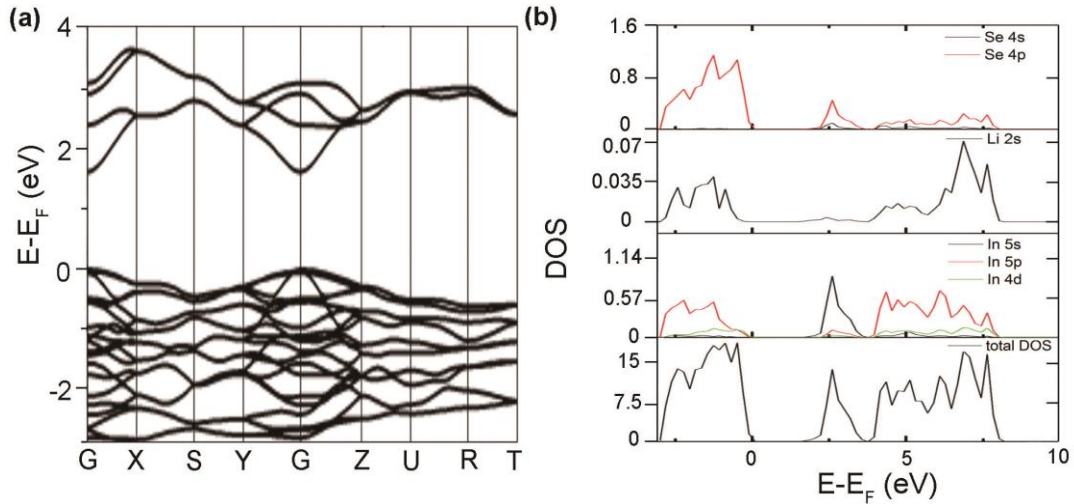


Figure 6. (a) Electronic structure of LiInSe₂; (b) Projected partial density of states of Li, In and Se and the total density of states.

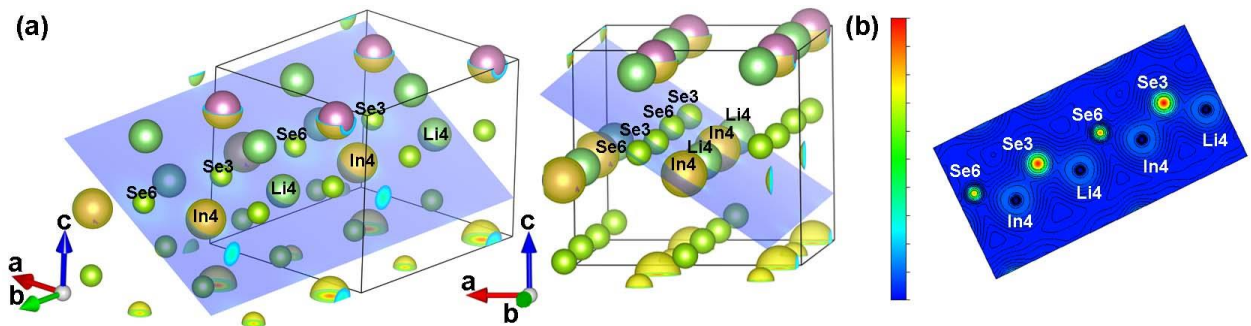


Figure 7. (a) The selected plane for calculation containing In–Se bonds and their nearest-neighbor Li atoms; (b) Electron density contour maps from $-4.6 \times 10^{-2} \text{ e}/\text{\AA}^3$ (blue) to $1.79 \text{ e}/\text{\AA}^3$ (red)

In addition, a contour plot in the plane containing In–Se bonds and their nearest-neighboring Li atoms with specific atom labels is shown in Figure 7a. The electron density distribution was calculated, as shown in Figure 7b. The areas, with gained electron density, are shown in red color, whereas the areas losing electron density are shown in blue color. It is clear from the contour that the Se3–In4 bonds have significant covalent character, while the Se6–In4 and Se6–Li4 bonds are prone to be more ionic in character. Because unlike covalent bonds, ionic bonds are not strongly directional, they allow ions to move more freely, leading to the formation of point defects. The anti-site defects of In_{Li} and Li_{In} , the main cause of various colors of LiInSe_2 crystals, might be related to the bonding state of Se6–In4.

Resistivity and Photoresponse

The electrical resistivity of LiSe-Y at room temperature is $6.1 \times 10^{11} \Omega \cdot \text{cm}$ fitted from the I-V curve, shown in Figure 8a. Such a high resistivity gives a low dark current and a high signal-to-noise ratio and allows for a higher applied bias to increase the charge collection efficiency. The resistivity of LiSe-R1 and LiSe-R2 are $1.7 \times 10^{12} \Omega \cdot \text{cm}$ and $8.1 \times 10^{11} \Omega \cdot \text{cm}$ respectively, shown in the Supporting Information.

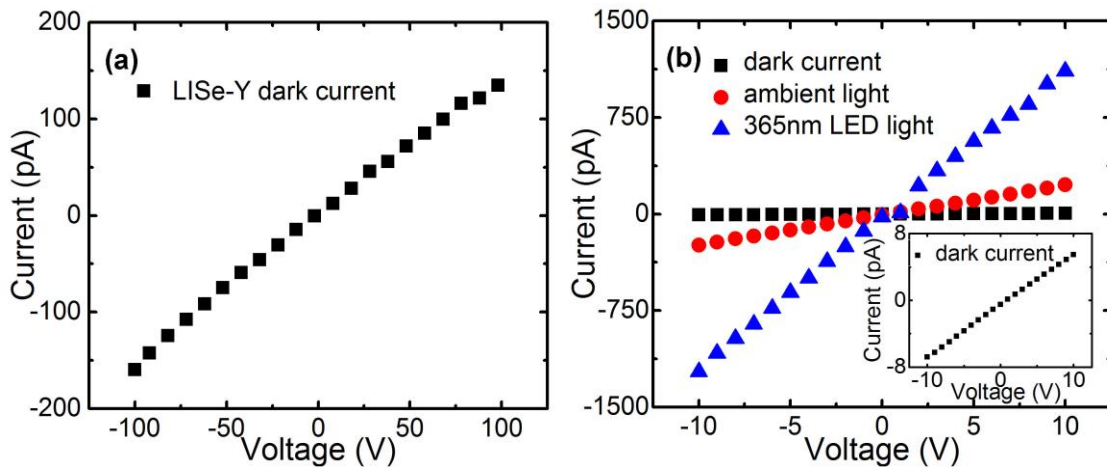


Figure 8. I-V curve under a bias of 100V in the dark (a); I-V curve of LiSe-Y in dark ambient (Inset of (b)) and under the illumination of ambient light or 365nm LED light (b)

The photoconductivity was evaluated under the illumination of ambient light ($\sim 50 \mu\text{W}\cdot\text{cm}^{-2}$) and 365 nm LED light ($\sim 1 \text{ mW}\cdot\text{cm}^{-2}$), shown in Figure 8b. Under an applied voltage of 10 V, the dark current was as low as 5.45 pA. When LISe-Y was subjected to room ambient light, it produced 40 times as much current, ~ 226 pA under 10 V bias. Under the illumination of 365 nm LED, the current was 1111 pA under a bias of 10 V, 200 times the dark current. The main reason of the difference between ambient light and LED 365 nm light is the different light intensity per unit area. This observation indicates that our LiInSe₂ crystals have a good photoconductivity.

Alpha Particles and γ -ray Response

Figure 9a shows the alpha particle response spectra for the obtained LiInSe₂ detectors of LISe-Y at various bias voltages. The photo-peak was clearly resolved in the spectra. The alpha particle response spectra of LISe-R2 and LISe-R1 are shown in Figure 9c and 9d.

Considering the limited range short incident depth ($\sim 20 \mu\text{m}$, this value is obtained in CdTe crystal calculated by the SRIM code) of alpha particles in the crystal³⁷⁻³⁹, the electron-hole pairs are generated in a shallow region near the surface. The spectroscopic response at different applied voltages allows us to evaluate the mobility-lifetime product of electron carriers with a modified methodology of single carrier Hecht equation⁴⁰. This method extracts the mobility-lifetime product from the analysis of charge collection efficiency (*CCE*) under various bias voltage applied. The *CCE* is written as:

$$CCE \approx \frac{\mu\tau V}{d^2} \left[1 - \exp\left(\frac{-d^2}{\mu\tau V}\right) \right] \quad (1)$$

where μ is carrier mobility, τ is carrier lifetime, V is the bias voltage, d is the thickness of sample, and *CCE* is proportional to the photo-peak centroid. The carrier mobility-lifetime products of these three wafers were estimated according to the Equation (1), shown in the Table 2. The

mobility-lifetime product of LISe-Y was fit across the range between 350 V and 1400 V, shown in Figure 9b. However, not all the wafers (especially for LISe-R1) can bear the high voltage of 1400V like LISe-Y. Therefore, we fit the mobility-lifetime product of LISe-R1 and LISe-R2 across a lower voltage range, shown in the insets of Figure 9c and 9d.

Table 2. The 5.48 MeV alpha particle response of as-grown crystal wafers

Wafer	Formula	E_g (eV)	Energy resolution	$\mu\tau_e$ (cm^2V^{-1})
LISe-R1	$\text{Li}_{1.04}\text{In}_{1.10}\text{Se}_2$	2.01	43.1%	$9.3 \pm 1.9 \times 10^{-6}$
LISe-R2	$\text{Li}_{0.99}\text{In}_{1.02}\text{Se}_2$	2.15	28.9%	$1.5 \pm 0.2 \times 10^{-5}$
LISe-Y	$\text{LiIn}_{1.06}\text{Se}_2$	2.83	23.3%	$2.5 \pm 0.2 \times 10^{-5}$

The energy resolution of these three wafers to a 5.48 MeV alpha particle varies from 43.1% to 23.3% with a mobility-lifetime product from 9.3×10^{-6} to $2.5 \times 10^{-5} \text{ cm}^2\text{V}^{-1}$. The performance variation is consistent with a lower electron mobility lifetime and a shorter drift mobility length, mainly ascribed to the deep level trapping centers.

According to Figure 9a and 9c, LISe-R2 and LISe-Y show a relatively narrow FWHM with an energy resolution of 28.9% and 23.3% respectively, which is better than the reported resolution of $\sim 38.2\%$ ²⁷. This is also in a good agreement with a higher electron mobility-lifetime product of $1.5\text{-}2.5 \times 10^{-5} \text{ cm}^2\text{V}^{-1}$ comparing with the reported product of $3\text{-}7.6 \times 10^{-6} \text{ cm}^2\text{V}^{-1}$ ^{116, 27}. These results confirm the good crystalline quality of LISe-R2 and LISe-Y and it is consistent with the closer stoichiometric ratio to the ideal LiInSe_2 which reduces the concentration of some specific component-associated defects of V_{Se} and Li_i ²⁴. The low charge collection efficiencies of LISe-R1 is possibly ascribed to the high density of grown-in defects associated with the deviation.

Additionally, LISe-Y displays the best response to alpha particles among the three wafers. A shift of the photo-peak centroid over a wide range of applied electric field is observed in Figure

9a, indicating a steady growth of charge collection efficiency. LISe-Y is a yellow crystal with an optical band gap of 2.83 eV listed in Table 2. The better response of the yellow LiInSe₂ crystal to ionizing radiation is attributed to the lower density of defects as compared to those in the red LiInSe₂ crystal⁴¹. The red color of LISe-R2 is attributed to anti-site defects of In_{Li} and Li_{In}, and these defects act as scattering and trapping centers deteriorating the charge carrier transport and degrading the performance of the red samples.

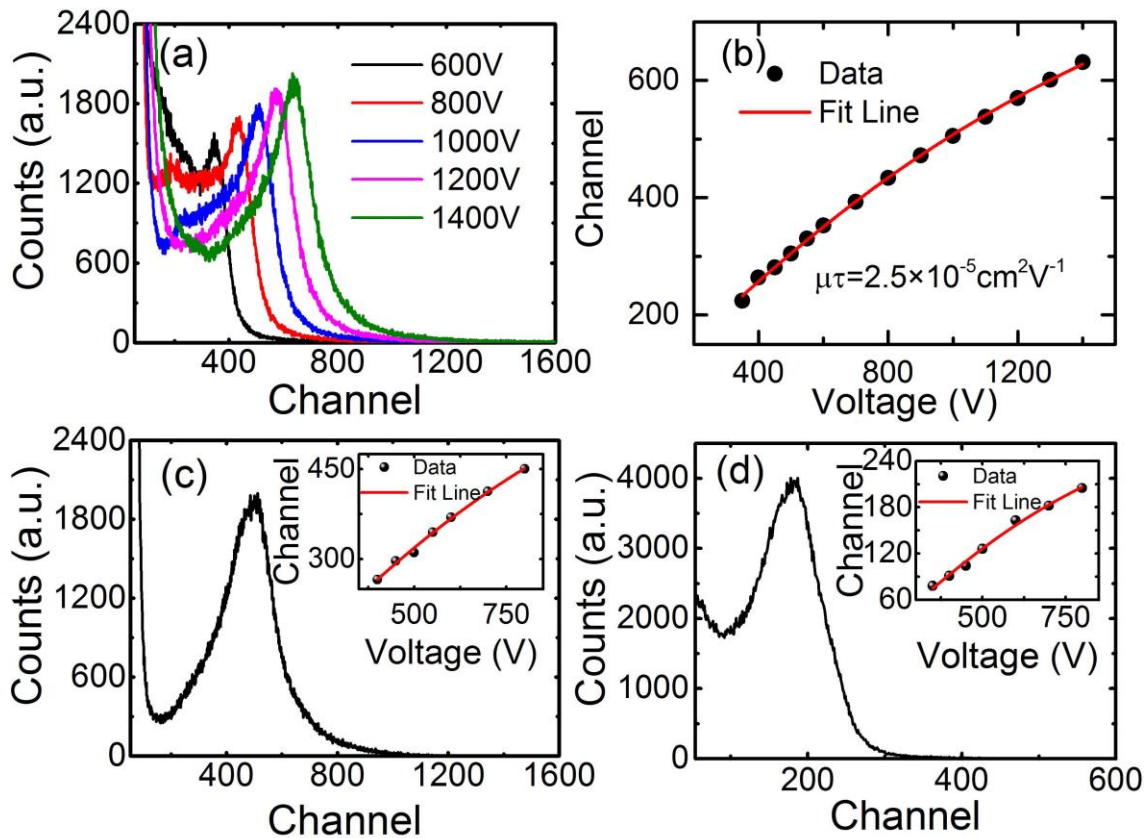


Figure 9. (a) Alpha particle pulse height spectra of LISe-Y as a function of bias voltage; (b) the full-energy peak vs applied voltage for LISe-Y. The line is the fitting result using Equation (1); (c) pulse height spectra of LISe-R2 at 1000 V and the inset is the plot of channel number vs voltage, and the fit line using Equation (1); (d) pulse height spectra of LISe-R1 at 500 V, and the inset is the plot of channel number vs voltage and the fit line using Equation (1).

Finally, LiInSe₂ samples show potentially good neutron/ γ discriminating performance, because no response to γ -rays was found when illuminated under a ⁶⁰Co@1.33MeV γ -ray source. This is because of the relatively low average atomic number of LiInSe₂ (Supporting Information).

Conclusion

Single crystal LiInSe₂, a promising candidate for neutron detectors, can achieve superior n/ γ discriminating performance and a high resistivity in the order of 10¹¹-10¹² Ω ·cm. Our low temperature synthesis method produces stoichiometric LiInSe₂ crystals, which suppresses the formation of Li vacancies. Such crystals exhibit electron mobility-lifetime product of $\sim 2.5 \times 10^{-5}$ cm²V⁻¹. A detector based on the yellow stoichiometric crystal, achieved an energy resolution of 23.3% when illuminated with a ²⁴¹Am@5.48MeV alpha source. This performance is better than that of the previously reported LiInSe₂ crystals²⁷. Further improvements on LiInSe₂ crystals are anticipated through improvements in the melt growth procedure which will further tailor the stoichiometry of the compound for continued development of neutron detectors based on semiconductors.

ASSOCIATED CONTENT

The following files are available free of charge.

Figure S1. Resistivity of LISe-R1 and LISe-R2. Figure S2. LISe-R2 response to (a) ²⁴¹Am@5.48MeV and (b) ⁶⁰Co@1.33MeV under the bias of 1000 V (PDF)

AUTHOR INFORMATION

Corresponding Author

E-mail: xyd220@nwpu.edu.cn (Yadong Xu)

E-mail: m-kanatzidis@northwestern.edu (Mercouri G. Kanatzidis)

ORCID

Yadong Xu: 0000-0002-1017-9337

Mercouri G. Kanatzidis: 0000-0003-2037-4168

ACKNOWLEDGMENT

This work has been financially supported by National Natural Science Foundations of China (U1631116, 51372205 and 51702271), National Key Research and Development Program of China (2016YFE0115200 and 2016YFF0101301), Natural Science Basic Research Plan in Shaanxi Province of China (2016KJXX-09) and the Fundamental Research Funds for the Central Universities (3102017zy057). This work was also supported in part by Laboratory Directed Research and Development (LDRD) funding from Argonne National Laboratory, provided by the Director, Office of Science, of the U.S. Department of Energy under contract No DE-AC02-06CH11357 (DYC, MGK).

REFERENCES

- (1) Kouzes, R. T. *The ³He supply problem*; No. PNNL-18388; Pacific Northwest National Laboratory: Richland, WA, 2009.
- (2) Cecil, R. A.; Anderson, B. D.; Madey, R. *Nucl. Instrum. Methods.* **1979**, 161, 439-447.

- (3) Van Eijk, C. W. E.; Bessière, A.; Dorenbos, P. *Nucl. Instrum. Methods Phys. Res., Sect. A* **2004**, 529, 260-267.
- (4) Kesanli, B.; Hong, K.; Meyer, K.; Im, H.; Dai, S. *Appl. Phys. Lett.* **2006**, 89, 214104.
- (5) Robertson, B. W.; Adenwalla, S.; Harken, A.; Welsch, P.; Brand, J. I.; Dowben, P. A.; Claassen, J. P. *Appl. Phys. Lett.* **2002**, 80, 3644-3646.
- (6) Nikolić, R. J.; Conway, A. M.; Reinhardt, C. E.; Graff, R. T.; Wang, T. F.; Deo, N.; Cheung, C. L. *Appl. Phys. Lett.* **2008**, 93, 133502.
- (7) Marinelli, M.; Milani, E.; Prestopino, G.; Scoccia, M.; Tucciarone, A.; Verona-Rinati, G.; Angelone, M.; Pillon, M.; Lattanzi, D. *Appl. Phys. Lett.* **2006**, 89, 143509.
- (8) McGregor, D. S.; Bellinger, S. L.; Shultis, J. K. *J. Cryst. Growth* **2013**, 379, 99-110.
- (9) McGregor, D. S.; Hammig, M. D.; Yang, Y. H.; Gersch, H. K.; Klann, R. T. *Nucl. Instrum. Methods Phys. Res., Sect. A* **2003**, 500, 272-308.
- (10) Isaenko, L.; Yelisseyev, A.; Lobanov, S.; Petrov, V.; Rotermund, F.; Slekyš, G.; Zondy, J. J. *J. Appl. Phys.* **2002**, 91, 9475.
- (11) Zondy, J. J.; Vedenyapin, V.; Yelisseyev, A.; Lobanov, S.; Isaenko, L.; Petrov, V. *Opt. Lett.* **2005**, 30, 2460-2462.
- (12) Marchev, G.; Tyazhev, A.; Vedenyapin, V.; Kolker, D.; Yelisseyev, A.; Lobanov, S.; Isaenko, L.; Zondy, J. J.; Petrov, V. *Opt. Express* **2009**, 17, 13441-13446.
- (13) Kargar, A.; Tower, J.; Hong, H.; Cirignano, L.; Higgins, W.; Shah, K. *Proc. SPIE* **2011**, 8142.

- (14) Tupitsyn, E.; Bhattacharya, P.; Rowe, E.; Matei, L.; Groza, M.; Wiggins, B.; Burger, A.; Stowe, A. *Appl. Phys. Lett.* **2012**, 101, 202101.
- (15) Wiggins, B.; Groza, M.; Tupitsyn, E.; Lukosi, E.; Stassun, K.; Burger, A.; Stowe, A. *Nucl. Instrum. Methods Phys. Res., Sect. A* **2015**, 801, 73-77.
- (16) Franks, L.; James, R. B.; Fiederle, M.; Burger, A.; Bell, Z. W.; Burger, A.; Matei, L.; Groza, M.; Stowe, A.; Tower, J.; Kargar, A.; Hong, H. *Proc. SPIE* **2015**, 9593.
- (17) Kamijoh, T.; Kuriyama, K. *J. Cryst. Growth* **1981**, 51, 6-10.
- (18) Isaenko, L. I.; Vasilyeva, I. G. *J. Cryst. Growth* **2008**, 310, 1954-1960.
- (19) Tupitsyn, E.; Bhattacharya, P.; Rowe, E.; Matei, L.; Cui, Y.; Buliga, V.; Groza, M.; Wiggins, B.; Burger, A.; Stowe, A. *J. Cryst. Growth* **2014**, 393, 23-27.
- (20) Wang, S.; Zhang, X.; Zhang, X.; Li, C.; Gao, Z.; Lu, Q.; Tao, X. *J. Cryst. Growth* **2014**, 401, 150-155.
- (21) Ma, T.; Zhu, C.; Lei, Z.; Yang, C.; Sun, L.; Zhang, H. *J. Cryst. Growth* **2015**, 415, 132-138.
- (22) Jia, N.; Wang, S.; Gao, Z.; Wu, Q.; Li, C.; Zhang, X.; Yu, T.; Lu, Q.; Tao, X. *Cryst. Growth Des.* **2017**, 17, 5875-5880.
- (23) Smith, C. J.; Lowe, C. W. *J. Appl. Phys.* **1989**, 66, 5102.
- (24) Li, Y.; Zhao, X.; Cheng, X. *J. Phys. Chem. C* **2015**, 119, 29123-29131.

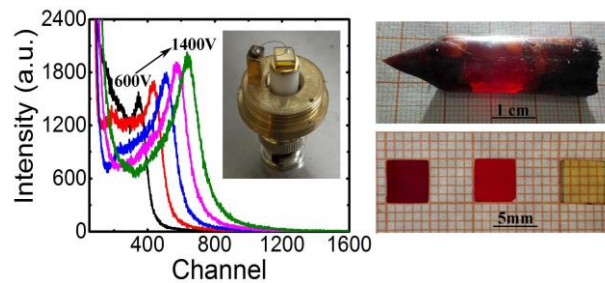
- (25) Cui, Y.; Bhattacharya, P.; Buliga, V.; Tupitsyn, E.; Rowe, E.; Wiggins, B.; Johnstone, D.; Stowe, A.; Burger, A. *Appl. Phys. Lett.* **2013**, 103, 092104.
- (26) Vijayakumar, P.; Magesh, M.; Arunkumar, A.; Anandha Babu, G.; Ramasamy, P.; Abhaya, S. *J. Cryst. Growth* **2014**, 388, 17-21.
- (27) Burger, A.; Franks, L.; James, R. B.; Fiederle, M.; Stowe, A. C.; Wiggins, B.; Bhattacharya, P.; Tupitsyn, E.; Groza, M.; Matei, L.; Stassun, K.; Herrera, E.; Lukosi, E.; Burger, A. *Proc. SPIE* **2014**, 9213.
- (28) Hultgren, R.; Desai, P. D.; Hawkins, D. T.; Gleiser, M.; Kelley, K. K.; Wagman, D. D. *Selected Values of Thermodynamic Properties of the Elements*; American Society for Metals: Metals Park, OH, 1973.
- (29) Ohse, R. W. *Handbook of Thermodynamic and Transport Properties of Alkali Metals*; Blackwell Scientific Publications: Oxford, UK, 1994.
- (30) Tauc, J. *Mater. Res. Bull.* **1968**, 3, 37-46.
- (31) Davis, E.; Mott, N. *Philos. Mag.* **1970**, 22, 0903-0922.
- (32) Kresse, G.; Hafner, J. *Phys. Rev. B* **1994**, 49, 14251.
- (33) Kresse, G.; Furthmüller, J. *Comput. Mater. Sci.* **1996**, 6, 15-50.
- (34) Kresse, G.; Furthmüller, J. *Phys. Rev. B* **1996**, 54, 11169.
- (35) Perdew, J. P.; Burke, K.; Ernzerhof, M. *Phys. Rev. Lett.* **1996**, 77, 3865.
- (36) Mori-Sánchez, P.; Cohen, A. J.; Yang, W. *Phys. Rev. Lett.* **2008**, 100, 146401.

- (37) Sellin, P.; Davies, A.; Lohstroh, A.; Ozsan, M.; Parkin, J. *IEEE Trans. Nucl. Sci.* **2005**, 52, 3074-3078.
- (38) Ruzin, A.; Nemirovsky, Y. *J. Appl. Phys.* **1997**, 82, 4166-4171.
- (39) Ziegler, J. F. *Nuclear Instruments and Methods in Physics Research Section B* **2004**, 219, 1027-1036.
- (40) Hecht, K. *Z. Phys.* **1932**, 77, 235-245.
- (41) James, R. B.; Fiederle, M.; Burger, A.; Franks, L.; Gueorguiev, A.; Hong, H.; Tower, J.; Kim, H.; Cirignano, L.; Burger, A.; Shah, K. *Proc. SPIE* **2016**, 9968.

For Table of Contents Use Only

Stoichiometric effects on the photoelectric properties of LiInSe₂ crystals for neutron detection

Lijian Guo, Yadong Xu, Hongjian Zheng, Wangqi Xue, Jiangpeng Dong, Binbin Zhang, Yihui He, Gangqiang Zha, Duck Young Chung, Wanqi Jie, Mercuri G. Kanatzidis



With the help of low temperature synthesis processing, stoichiometric deviation is reduced and stoichiometric crystals are obtained. Stoichiometric LiInSe₂ crystals grown by vertical Bridgman method exhibited high resistivity of 10^{11} - 10^{12} $\Omega\cdot\text{cm}$ and a direct band gap of 2.01 eV - 2.83 eV. The yellow stoichiometric crystal achieves an energy resolution of 23.3% for alpha particles of ²⁴¹Am@5.48MeV.

Supporting Information

Stoichiometric effects on photoelectric properties of the as-grown LiInSe₂ crystal for neutron detector

Lijian Guo^{1, 2, 3}, Yadong Xu^{1, 2, 3}, Hongjian Zheng^{1, 2}, Wangqi Xue^{1, 2}, Jiangpeng Dong^{1, 2}, Binbin Zhang^{1, 2}, Yihui He³, Gangqiang Zha^{1, 2}, Duck Young Chung⁴, Wanqi Jie^{1, 2}, Mercuri G. Kanatzidis^{3, 4}*

¹State Key Laboratory of Solidification Processing, and ²Key Laboratory of Radiation Detection Materials and Devices, Northwestern Polytechnical University, Xi'an 710072, China

³Department of Chemistry, Northwestern University, Evanston, IL 60208, USA

⁴Materials Science Division, Argonne National Laboratory, Argonne, IL 60439, USA

Resistivity

Usually, it is believed that the crystal with high resistivity enjoys lower leakage current, which can decrease background noise and improve signal-noise ratio. The resistivity of LISe-R1 and LISe-R2 are about $1.7 \times 10^{12} \Omega \cdot \text{cm}$ and $8.1 \times 10^{11} \Omega \cdot \text{cm}$ respectively in dark environment, shown in Figure S1.

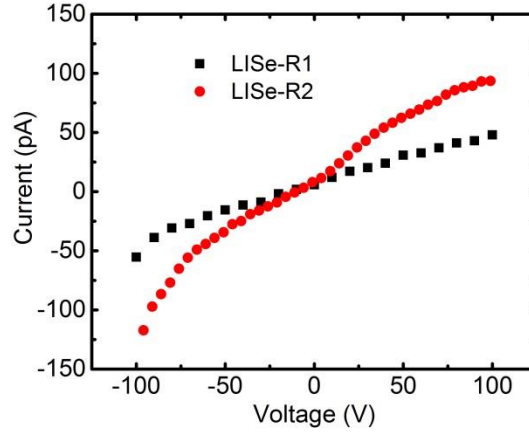


Figure S1. Resistivity of LISe-1601 and LISe-1602

Carrier mobility

Carrier mobility is a significant parameter of detector performance. In our work, it is estimated by using the risetime t_r of transient waveforms from the preamplifier under a $^{241}\text{Am}@5.48\text{MeV}$ source, which is a common method to estimate the carrier mobility of insulating materials. The drift time of photo-generated carriers across the thickness is given by

$$\mu = \frac{d^2}{U t_r} \quad (1)$$

where U is the applied bias across the thickness d , and t_r is the transit time of the carriers across the sample.

Figure S2(a) shows the risetime of LISe-Y as a function of electrical field. The electron mobility according to equation (1) is $255 \text{ cm}^2 \text{V}^{-1} \text{s}^{-1}$.

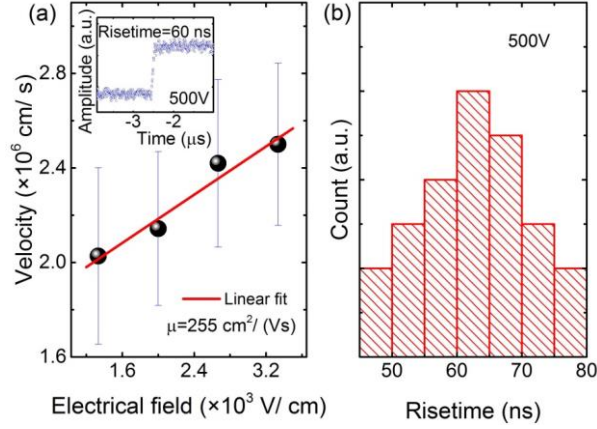


Figure S2. (a) Risetime of LISe-Y as a function of electrical field; (b) The distribution of electron risetime under 500V bias.

LiInSe₂ crystal response to γ ray

In view of neutron beam usually accompanied with high energy γ ray, it is necessary to measure n/ γ discriminating property of LiInSe₂. The noise background was obtained firstly after 12-hours' counting without illuminated by radiation source. Then the wafer was illuminated by ⁶⁰Co. And the response spectrum was collected for 4, 8 and 12 hours respectively. As is seen in Figure S3(b), there was no obvious difference among 4, 8 and 12 hours-counting results from channel 100. And the 12-hours spectrum is closed to the background when the wafer was illuminated by ⁶⁰Co. As a result, compared with the high counts of alpha particles, LiInSe₂ crystal exhibits a dull response to γ ray which should be ascribed to the low absorption cross section of γ ray for LiInSe₂ crystal. According to the equation written below

$$\tau_a = AZ^5(h\nu)^{-\frac{7}{2}} \quad (2)$$

where τ_a is photoelectric absorption cross section, A is a constant, Z is the atomic number of absorption material and $h\nu$ is the energy of photon. The photoelectric absorption cross section is

determined by average atomic number and incidence photon energy mainly. The average atomic number of LiInSe₂ crystal decrease hugely because of light element Li.

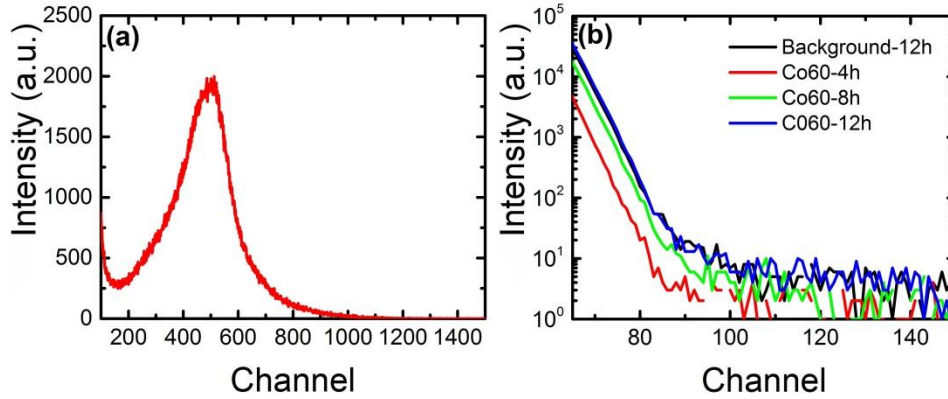


Figure S3. LInSe-1602 response to ²⁴¹Am@5.48 MeV (a) and ⁶⁰Co@1.33MeV (b) under the bias of 1000V

On the basis of experiment result, LiInSe₂ crystal is insensitive to γ photons of 1.33 MeV. According to equation (2), LiInSe₂ crystal will be also dull to those γ photons whose energy is higher. On the other hand, although the photoelectric absorption cross section of lower energy photon (<1.33 MeV) is higher, the resolution of 23.3% is enough to distinguish the signal from the lower energy photon and the triton and alpha particles of 2-3 MeV produced by the nuclear reaction ${}^6\text{Li}(n,\alpha){}^3\text{H}$.